Analytical and numerical study of direct and indirect combustion noise through a subsonic nozzle

Ignacio Duran, Stéphane Moreau, Thierry Poinsot

Analytical and numerical study of direct and indirect combustion noise through a subsonic nozzle

Ignacio Durán [1]
Snecma, 77550 Moissy-Cramayel, France - CERFACS, 31057 Toulouse, France

Stéphane Moreau [2]
Université de Sherbrooke, Sherbrooke, QC J1K2R1, Canada

Thierry Poinsot [3]
Institut de Mécanique des Fluides de Toulouse, 31400 Toulouse, France

Two mechanisms control sound generated by combustion in a gas turbines: direct combustion noise, in which acoustic waves generated by the flame propagate from the combustion chamber to the outlet through the turbine stages, and indirect combustion noise (or entropy noise), in which entropy waves created by unsteady combustion generate noise as they are accelerated through the turbine stages. These mechanisms can be studied in laboratories by sending acoustic and entropy waves through a nozzle as done in the EWG experiment of DLR [1]. Previous studies have addressed the case where the EWG nozzle is choked and have demonstrated that indirect noise was large compared to direct noise, suggesting that indirect noise only could be retained for gas turbine studies. In the present study, subsonic cases (where the nozzle is unchoked) are analysed using first a full numerical resolution of the unsteady Euler equations, second an analytical method based on the work of Marble and Candel [2] in the low frequency limit and finally the one-dimensional linearized Euler equations in the frequency domain. Results show that direct noise cannot be neglected in these situations and will have to be included for real gas turbines where the flow remains

---

[1] PhD Student, CFD Team; duran@cerfacs.fr
[2] Professor, GAUS, Mechanical Engineering Department, AIAA lifetime member
[3] Research Director, AIAA Associate Fellow

mostly subsonic.

Nomenclature

Latin letters

c	Fluid mean sound speed
C_p	Heat capacity at constant pressure
d	Characteristic slope length of the heating device
f	Frequency
i	Imaginary unit ($i^2 = -1$)
L^-	Entering wave at the outlet boundary
l_h	Heating device length
L_n	Nozzle length
L_{in}	Length of the inlet domain of the nozzle
L_{out}	Length of the exit domain downstream the nozzle throat
M	Mach number
m	Mass flow rate
p	Fluid pressure
P^+	Acoustic wave propagating downstream
P^-	Acoustic wave propagating upstream
p_2	Outlet pressure
p_{ref}	Reference static pressure at the outlet
Q'	Fluctuating heat release of the heating device
q'	Dimensionless fluctuating heat release of the heating device

R_1 Reflection coefficient at the inlet of the EWG nozzle, phase-shifted to the nozzle throat

R_2 Reflection coefficient at the outlet of the EWG nozzle, phase-shifted to the nozzle throat

R_{in} Reflection coefficient at the inlet of the experimental configuration

R_{out} Reflection coefficient at the outlet of the experimental configuration

R_{sc} Reflection coefficient at the inlet of the settling chamber

s Fluid entropy

S_0 Cross-section area of the nozzle inlet

S_{sc} Cross-section area of the Settling chamber

t Time

t_0 Time of the heating device triggering

T_p Heating device's pulse duration

T_t Fluid total temperature

u Fluid velocity

x Axial coordinate of the nozzle

x_{hd} Heating device location

Greek Letters

Δt Time step of the numerical simulation

η Indirect to direct noise ratio

Γ Cross-section area ratio ($= S_0/S_{sc}$)

γ Specific heats ratio

κ Relaxation coefficient on pressure at the outlet boundary condition

λ Characteristic wavelength of the acoustic perturbations

Ω Dimensionless frequency

ω Angular frequency

$\phi(t)$ Temporal variation of the electrical device source term

$\phi(x,t)$ Source term in the energy equation

Φ_0 Amplitude of the source term in the energy equation

ρ Fluid mean density

σ Entropy wave

τ Relaxation time of the heating device pulse model

I. Introduction

Noise emissions are a major issue for aircraft and engines manufacturers due to the proximity of airports to residential zones and to the increasing international noise regulations defined by the ICAO. During the last decades, research efforts allowed a significant reduction of jet, fan and external aerodynamic noise which must be continued in order to meet future regulations. The reduction of these sources has increased the relative influence of other noise sources in the aircraft. For these sources the possible reduction is relatively high, as physical mechanisms governing them are not yet fully understood. One of these sources is combustion noise, which is generated by heat fluctuations induced by the turbulent flame. These fluctuations generate acoustic but also entropy waves that propagate through the turbine stages to reach the outlet of the engine, contributing to the global engine noise.

Two mechanisms of combustion noise generation can be identified [2]: direct combustion noise, which is due to acoustic waves created in the combustion chamber that propagate through the turbine stages, and indirect noise, which appears when entropy waves (hot spots) are accelerated through the turbine. The acceleration of these entropy waves generates pressure fluctuations that propagate upstream (contributing to combustion instabilities when a positive feedback occurs), and downstream from the turbine stage (generating indirect combustion noise, as shown in [2, 3]). Both mechanisms of combustion noise generation were identified by Marble and Candel [2] using the linearized Euler Equations (LEE) and an analytical method to solve the propagation

equations considering a quasi-1D configuration, based on the compact nozzle hypothesis. This hypothesis was used to extend the analytical method to a 2D configuration of a turbine stage (Cumpsty and Marble [4]). The study of combustion noise is directly linked to the propagation of acoustic and entropy waves through the turbine stages, where the mean flow is accelerated and decelerated repeatedly. While the propagation of noise in unconfined domains has been studied in depth [5–8], no acoustic analogy exists for the propagation of acoustic and entropy waves through turbo-machinery. One and two-dimensional models of wave propagation must be used to propagate the noise generated in the combustor to the outlet of the engine. Waves generated in the combustion chamber can be simulated using advanced Large Eddy Simulations (LES) and the noise at the outlet can be predicted by combining them with these analytical models of waves propagation [4]. This can be done without having to combine LES results and a turbine stage to simulate the combustion chamber, which would be extremely CPU demanding.

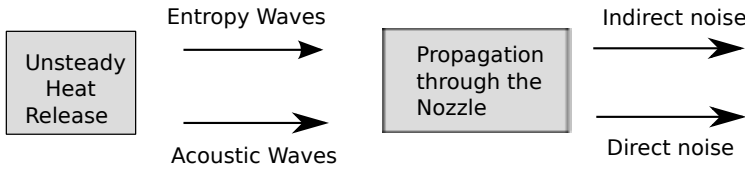

Fig. 1 The two mechanisms of combustion noise generation: Direct noise and indirect noise.

Leyko *et al.* [9] used one-dimensional analytical methods combined with numerical tools to show that the ratio of indirect to direct combustion noise is high in actual aero-engines, but low in most laboratory combustion chambers because most chambers in laboratories operate at atmospheric pressure without exhaust nozzle, and are not followed by a mean flow acceleration. One exception is the experiment of Bake *et al.* [1] that intended to specifically focus on indirect combustion noise. This experiment, called the Entropy Wave Generator (EWG), was used by Leyko *et al.* [10] to validate the analytical tools created by Marble and Candel [2] in the choked supersonic case [11, 12], showing that indirect combustion noise can be correctly predicted using the analytical method. The present work focuses on the subsonic cases to explain the mechanisms generating noise in the experience and to analyse the compact nozzle hypothesis in this case. In Section II the experimental configuration

of the EWG experiment is described, as well as an analysis of the boundary conditions and a consideration about the heating device. A numerical simulation of the complete set-up is performed in Section III A, the analytical method of Marble and Candel [2] is briefly outlined and applied to the experimental subsonic data in Section III B. The variant proposed by Bake *et al.* [13] is also outlined. A study of the limits of the compact nozzle hypothesis is presented in Section III C and a semi-analytical approach using the linearized Euler equations through the nozzle is then proposed. Results obtained with all these methods are presented in Section IV and compared to experiments performed by Bake *et al.* [13]. Finally conclusions are presented in Section V.

II. The EWG experiment

The experiment performed by Bake *et al.* [1] at the DLR consists of a convergent-divergent nozzle with an electrical heating device placed at the inlet as sketched in Fig. 2 (geometrical parameters are summarized in Table 1). Depending on the mass flow rate the operating conditions can be varied from unchoked to choked flow with various exit Mach numbers, including supersonic flow. Leyko *et al.* [10] and Mühlbauer *et al.* [14] studied the supersonic case (with a normal shock after the choked nozzle). The present study is therefore restricted to the unchoked subsonic configuration, using mainly Reference Test Case 2 of [1], summarized in Table 2 .

Convergent Length	Divergent Length	Inlet Diameter	Outlet Diameter	Throat Diameter
13mm	250mm	30mm	40mm	7.5mm

Table 1 Geometric characteristics of the nozzle of the experimental set-up.

Inlet Mach number	Throat Mach Number	Outlet Mach number	Inlet Pressure	Outlet Pressure
0.033	0.7	0.01861	105,640Pa	101,300Pa

Table 2 Physical parameters of the subsonic case (Reference Test Case 2).

The mean steady flow is perturbed with a temperature pulse (Fig. 3) generated electrically by

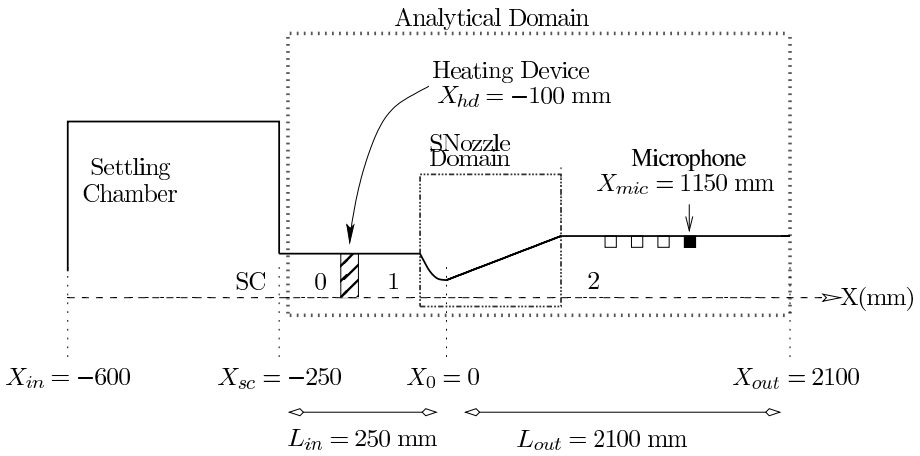

Fig. 2 Sketch of the EWG considered for the numerical simulations, with the definition of the analytical and the SNozzle domains, the sections where the different variables will be calculated: SC (settling chamber section at X_{sc}), 0 (inlet duct section at X_{sc}), 1 (inlet nozzle section) and 2 (exit nozzle section), and the four microphones at the exit.

the heating device (located 100 mm upstream the nozzle throat) with a period of 1 second and a duration of 0.1 s. The acoustic waves generated are measured using four microphones placed at different sections at the outlet, shown in Fig. 2. For the present study, the microphone placed at a distance of 1150 mm downstream from the nozzle throat will be used to compare analytical and numerical results with the experiment.

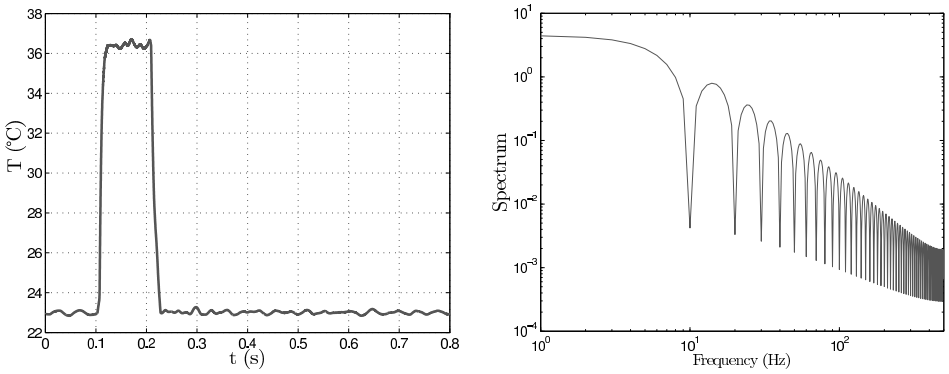

Fig. 3 Experimental temperature pulse induced by the heating device. Left: time signal. Right: Fourier transform of the time signal.

III. Simulations of the EWG experiment

To understand the mechanisms of noise generation analytical and numerical tools are used to reproduce the pressure signal captured by the microphone placed at the outlet of the experimental device. First a full Euler simulation of the entire set-up is performed (Section III A). The analytical method of Marble and Candel [2], based on the compact nozzle hypothesis, is then used to obtain a fully analytical solution of the problem (Section III B). This approach allows the separation of direct and indirect sources but is limited to low frequencies because of the compactness assumption. To study the validity of this hypothesis, a code called SNozzle (a solver for the linearized Euler equations in the frequency domain) is finally used (Section III C). Table 3 summarizes the three methods used and delimits the considered domain in each case.

Method	Type	Domain
Method A	Numerical Simulation	$X = X_{in}$ to $X = X_{out}$
Method B	Analytical Method	$X = X_{sc}$ to $X = X_{out}$
Method C	quasi-1D linearized Euler equations	$X = X_{sc}$ to $X = X_{out}$

Table 3 Three methods used to study the EWG.

A. Numerical simulations

Numerical simulations are performed using a two-dimensional axisymmetric mesh for the unsteady compressible Euler equations expressed in the conservative form [15]. The singularity on the axis has been removed by considering a small cylinder on which a slip condition is applied. The final mesh of the actual EWG nozzle geometry, shown in Fig. 4 has approximately 10000 nodes with 1000 nodes in the axial direction and 10 in each section, which was shown to yield simulations independent of the grid size. 3D effects were shown to be negligible in this case [10], and an axisymmetric mesh is enough to capture the noise generated by the heating device completely. The discretized geometry takes into account the complete nozzle, including the settling chamber (full domain plotted in Fig. 2, from X_{in} to X_{out}). The maximum mesh size is 1 mm, enough to resolve the temperature pulse accurately. The Lax-Wendroff scheme is used to solve the Euler equations using the AVBP code [15]. In [12] this scheme was shown to handle the present temperature gra-

dients correctly on the above fine grid. No significant differences have been seen with higher order Taylor-Galerking schemes. No viscosity, turbulence or boundary layers are taken into account in order to isolate the noise generation of the heating device from other possible sources.

Fig. 4 Zoom on the nozzle mesh.

1. Reflection coefficients

Boundary conditions in the EWG experiment are not anechoic: Leyko *et al.* [10] and Mühlbauer *et al.* [14] show that reflecting conditions should be considered at the experiment outlet to mimic the set-up correctly. The reflecting properties of the experiment were measured at the experimental outlet [14] and it was found that they can be modelled using a first order filter, namely,

$$R_{out} = \frac{-1}{1 + 2\imath\omega/\kappa} \quad . \tag{1}$$

This boundary condition is imposed in the following analytical model at a distance l_{out} of the nozzle. Tuning l_{out} and κ is sufficient to reproduce the correct boundary condition [16]. This was done by Leyko *et al.* [10] for the supersonic case, obtaining $\kappa = 160\ s^{-1}$ and $l_{out} = 2100$ mm measured from the nozzle throat. The outlet reflection coefficients are plotted in Fig. 5 of [10], where the experimental data is compared with the first order filter obtaining a good agreement for the frequency range of interest.

In the computation, the boundary condition given by Eq. (1) is introduced using non-reflecting boundary conditions (Poinsot and Lele [17]). Selle et al. [16] showed that the above reflection coefficient can be retrieved in the simulation by imposing the incoming waves as a function of the difference between the local and the reference pressures, namely,

$$L^- = 2\kappa\Delta t(p_{ref} - p)/(\rho c) \quad , \tag{2}$$

where ρ is the density and c the sound speed. When considering $\kappa = 0$ the boundary is completely non-reflecting, and when $\kappa \to \infty$ waves are completely reflected. For any intermediate value, the boundary condition acts as the first order filter given in Eq. (1), [18]. The above value of $\kappa = 160\ s^{-1}$ is used to mimic the experimental reflection coefficient. To impose the boundary condition at the correct distance l_{out} from the nozzle throat, the computational domain is extended to the appropriate length ($X_{out} = l_{out}$).

As the computational domain takes into account the settling chamber, the only inlet condition to impose corresponds to the inlet of the settling chamber ($X = X_{in}$) where a fully reflective inlet ($R_{in} = 1$) is used.

2. Heating device

The heating device is computed as a source term in the energy equation. The energy is distributed spatially,

$$\phi(x,t) = \Phi_0 \frac{1}{2}\left[\tanh\left(\frac{x - x_{hd} + l_h/2}{d}\right)\tanh\left(-\frac{x - x_{hd} - l_h/2}{d}\right) + 1\right]\phi(t) \quad , \tag{3}$$

where $x_{hd} = -100$ mm is the heating device location, $l_h = 60$ mm the heating device length, $d = 4$ mm a characteristic slope length and $\phi(t)$ the temporal fluctuation of the source term, given by an analytical function approximating the pulse generated, as done by Leyko *et al.* [10],

$$\phi(t) = \begin{cases} 1 - \exp(\frac{t-t_0}{\tau}) & \text{if } t \in [t_0, t_0 + T_p] \\ \\ \phi(t_0 + T_p)\exp(-\frac{t-t_0}{\tau}) & \text{if } t > t_0 + T_p \end{cases} , \tag{4}$$

where $t_0 = 100$ ms is the triggering time, $T_p = 100$ ms the pulse duration and τ the relaxation time of the pulse, set to 7 ms in our case. The comparison of the experimental and the analytical temperature pulse is shown in Fig. 5.

The comparison of numerical simulations with the experimental data (Fig. 6) shows that the evolution of pressure at the microphone placed 1150 mm downstream the nozzle is reasonably

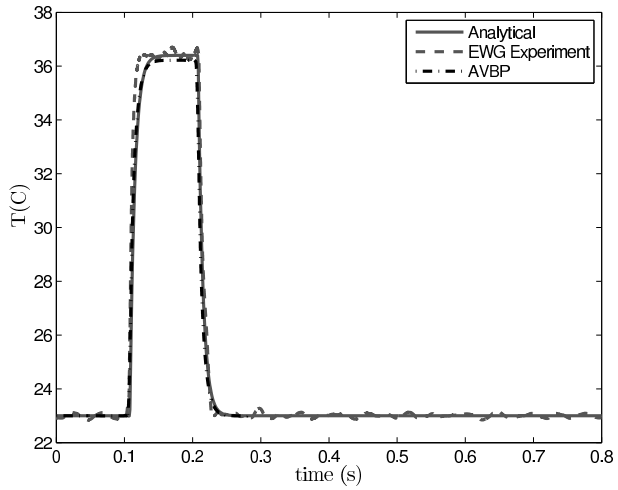

Fig. 5 Experimental temperature pulse induced by the heating device. Analytical function modelling the temperature signal compared to the EWG experimental data.

captured. The peak values of the signal are slightly overpredicted (a similar accuracy is found in Fig. 6 of [12]). To obtain a better match in the shape, a more detailed model for the outlet reflection coefficient should be used instead of a first order filter modelization.

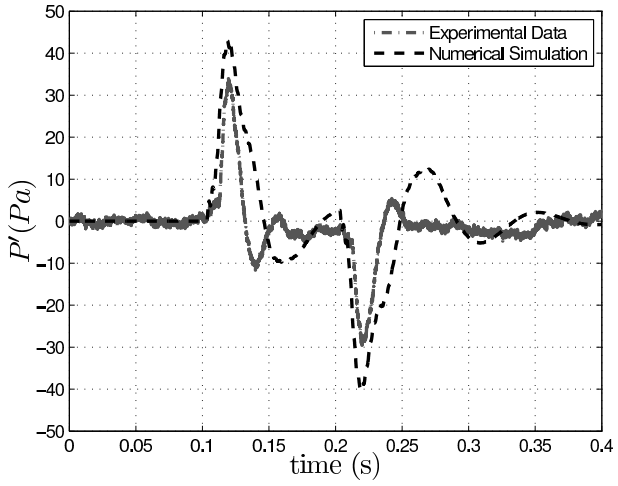

Fig. 6 Numerical simulation pressure signal compared to experimental data from the EWG.

B. Analytical Method

The analytical approach aims at calculating the noise produced by the EWG using the analytical domain plotted in Fig. 2, from X_{sc} to X_{out}. The method is based on the derivation of

jump conditions determining acoustic wave amplitudes at three locations: (0) and (1) upstream and downstream the heating device and (2) the outlet of the nozzle (at X_{out}) as shown in Fig. 2.

1. Heating device

Analytical methods are based on the decomposition of the source term in entropy and acoustic waves generated by the heating device. A simple 1D model can be used in the configuration illustrated in Fig. 7 to quantify the waves amplitudes: it takes into account the fluctuating heat release of the heating device Q', the acoustic and entropy waves (P^+, P^- and σ) and the mean flow. It should be noticed that the mean flow is constant through the device, and therefore $M_0 = M_1$.

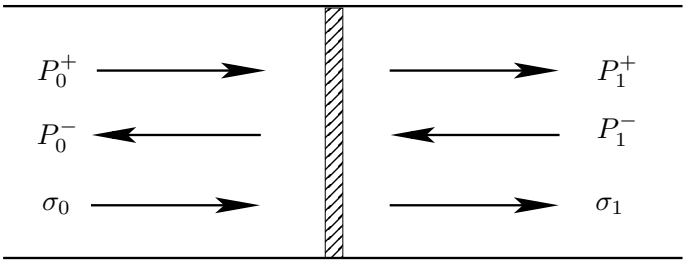

Fig. 7 Wave definition through the heating device.

As the heating device is short compared to all wavelength, the compact assumption used by Leyko *et al.* [9] states that the wavelength of the perturbations is long compared to the heating device length, and therefore perturbations of mass, temperature and entropy are transmitted from one side to the other of the heating device without any time delay. Considering negligible mean heat release ($Q \simeq 0$), the conservation equations of mass enthalpy and entropy can be written between both sides of the heating device as a jump condition, namely,

$$\left(\frac{\dot{m}'}{\dot{m}}\right)_0 = \left(\frac{\dot{m}'}{\dot{m}}\right)_1 \quad , \tag{5}$$

$$\left(\frac{T_t'}{T_t}\right)_0 + q'\left(1+\frac{\gamma-1}{2}M_0^2\right)^{-1} = \left(\frac{T_t'}{T_t}\right)_1 \quad , \tag{6}$$

$$\left(\frac{s'}{C_p}\right)_0 + q' = \left(\frac{s'}{C_p}\right)_1 \quad , \tag{7}$$

where $q' = Q'/(\dot{m}_0 C_p T_0)$ is a dimensionless form of the fluctuating heat release, s' is the entropy

fluctuation, C_p is the specific heat capacity and γ the heat capacity ratio. Using isentropic relations, the ideal gas law, and writing the mass flow as $\dot{m} = \rho A u$, the mass, total temperature and entropy equations can be expressed as a function of the primitive variables, namely,

$$\frac{\dot{m}'}{\dot{m}} = \frac{1}{M}\frac{u'}{c} + \frac{p'}{\gamma p} - \frac{s'}{C_p} \quad , \tag{8}$$

$$\frac{T_t'}{T_t} = \frac{1}{1+[(\gamma-1)/2]M^2}\left[(\gamma-1)M\frac{u'}{c} + (\gamma-1)\frac{p'}{\gamma p} + \frac{s'}{C_p}\right] \quad , \tag{9}$$

$$\frac{s'}{C_p} = \frac{p'}{\gamma p} - \frac{\rho'}{\rho} \quad , \tag{10}$$

where non-primed variables u, p, ρ and c represent the mean flow velocity, pressure, density and sound speed respectively, and primed variables represent small fluctuations of speed u', pressure p' and density ρ'.

Equations (5)-(7) have to be written as a function of the waves shown in Fig. 7 to impose the boundary conditions properly. The amplitudes of these waves (P^+, P^- and σ) are written as a function of the primitive variables as,

$$P^+ \equiv \frac{1}{2}\left[\frac{p'}{\gamma p} + \frac{u'}{c}\right] \quad , \tag{11}$$

$$P^- \equiv \frac{1}{2}\left[\frac{p'}{\gamma p} - \frac{u'}{c}\right] \quad , \tag{12}$$

$$\sigma \equiv \frac{s'}{C_p} = \frac{p'}{\gamma p} - \frac{\rho'}{\rho} \quad . \tag{13}$$

corresponding to the upstream and downstream propagating acoustic waves and the entropy wave, which propagate at speeds $u+c$, $u-c$ and u respectively (Fig. 7). Using Eqs.(8)-(10) into Eqs.(5)-(7), three relations between the known and unknown waves amplitudes are obtained,

$$(1+\frac{1}{M_1})P_0^+ + (1-\frac{1}{M_1})P_0^- - \sigma_0 = (1+\frac{1}{M_1})P_1^+ + (1-\frac{1}{M_1})P_1^- - \sigma_1 \quad , \tag{14}$$

$$\left[(1+M_1)P_0^+ + (1-M_1)P_0^- + \frac{\sigma_0+q'}{\gamma-1}\right] = \left[(1+M_1)P_1^+ + (1-M_1)P_1^- + \frac{\sigma_1}{\gamma-1}\right] \quad , \tag{15}$$

$$\sigma_0 + q' = \sigma_1 \quad . \tag{16}$$

To obtain the waves generated by the heating device the incoming waves (P_0^+, σ_0, P_1^-) are set to zero, so that the out-coming ones are caused by the effect of the heating device only ($\sigma_1 = \sigma_h$, $P_1^+ = P_h^+$, $P_0^- = P_h^-$). They read:

$$\sigma_h = q' \quad , \tag{17}$$

$$P_h^+ = \frac{M_1}{2(M_1+1)} q' \quad , \tag{18}$$

$$P_h^- = \frac{M_1}{2(1-M_1)} q' \quad , \tag{19}$$

where the subscript h denotes the wave generated by the effect of q' directly. Eqs. (17)-(19) show that the heating device generates stronger entropy waves than acoustic ones when considering low Mach numbers (by a ratio σ_h / P_h^+ of approximately 60 for the EWG case: $M_1 = 0.033$). Yet the contribution of direct noise at the outlet cannot be neglected without first considering a propagation model.

2. Reflection coefficients

To correctly model the propagation of waves through the EWG, the reflection coefficients have to be studied. The upstream reflection coefficient at the nozzle throat section ($X = X_0$) is noted R_1, and the downstream reflection coefficient is noted R_2 (Fig. 8).

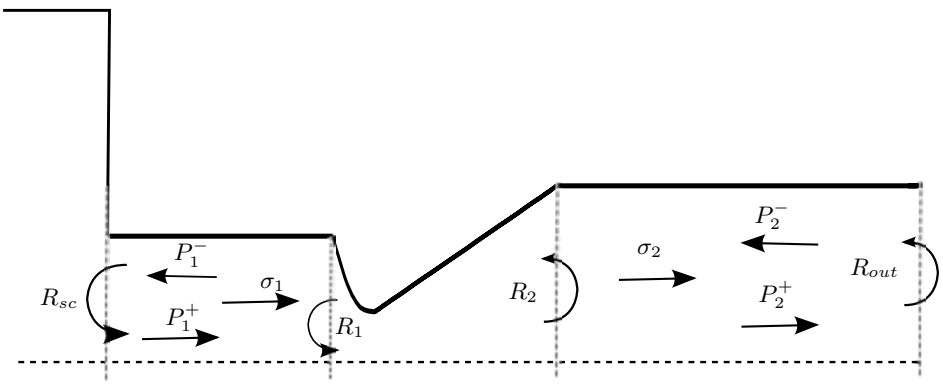

Fig. 8 Acoustic and entropy waves at the nozzle inlet and outlet in a subsonic nozzle. Waves are reflected in the boundary conditions R_{sc} and R_{out}.

The outlet reflection coefficient (R_2) is obtained by shifting (by a distance L_{out}) the reflection

coefficient at the outlet of the numerical simulation, R_{out} of Eq. (1) to section X_0. R_2 is written,

$$R_2 = \frac{P_2^-}{P_2^+} = \frac{P_{out}^- \exp\left(-2\pi i f \frac{L_{out}}{c_2(1-M_2)}\right)}{P_{out}^+ \exp\left(+2\pi i f \frac{L_{out}}{c_2(M_2+1)}\right)} = R_{out} \exp\left(-2\pi i f \frac{L_{out}}{c_2(M_2+1)}\right) \exp\left(-2\pi i f \frac{L_{out}}{c_2(1-M_2)}\right), \tag{20}$$

where $L_{out} = 2100$ mm is the same distance used for the numerical simulation. Similarly, the inlet reflection coefficient R_1 can be written as a function of the reflection coefficient at X_{sc}, R_{sc}, shifted by L_{in},

$$R_1 = R_{sc} \exp(-2\pi i f \frac{L_{in}}{c_1(M_1+1)}) \exp(-2\pi i f \frac{L_{in}}{c_1(1-M_1)}) \quad , \tag{21}$$

where $L_{in} = 250$ mm is the distance between the settling chamber outlet (X_{sc}) and the nozzle throat (X_0). For both cases the effect of the Mach number is retained for the propagation, though for low Mach numbers it can be neglected, obtaining the same equations as in [10]. The reflection coefficient R_{sc} must be modelled. In the supersonic case Leyko *et al.* [10] tried both $R_{sc} = 0$ and $R_{sc} = -1$, showing that it had little influence on the results. For the present subsonic cases however, the settling chamber must be modelled as it is supposed to have a stronger effect on the results. In fact, as the flow is subsonic, waves can propagate upstream from the nozzle divergent section, reflect on the inlet at X_{sc} and propagate downstream, interacting again with the nozzle and contributing to the global noise. Unfortunately, no experimental data exist for this reflection coefficient. An analytical approximation is proposed here to take into account the settling chamber. The conservation equations across the section change at X_{sc} between the settling chamber (SC) and the inlet duct (0) before the heating device (Fig. 2) can be written,

$$S_{sc} \cdot u'_{sc} = S_0 \cdot u'_0 \quad , \tag{22}$$

$$p'_{sc} = p'_0 \quad , \tag{23}$$

considering low Mach number both at the settling chamber and at the nozzle inlet. In this way, two relations can be written between the waves at the settling chamber and at the heating device tube, namely,

$$P_{sc}^+ - P_{sc}^- = \Gamma(P_0^+ - P_0^-) \quad , \tag{24}$$

$$P_{sc}^+ + P_{sc}^- = P_0^+ + P_0^- \quad , \tag{25}$$

where $\Gamma = \frac{S_0}{S_{sc}}$ is the ratio between sections. R_{sc} is defined as the relation between the downstream propagating wave and the upstream propagating one in section X_{sc}. This gives,

$$R_{sc} = \frac{P_0^+}{P_0^-} = \frac{(\Gamma - 1) + R_{in}(\Gamma + 1)}{(\Gamma + 1) + R_{in}(\Gamma - 1)} \quad . \tag{26}$$

where R_{in} is the reflection coefficient at the inlet of the settling chamber (X_{in}) phase-shifted to X_{sc} using the length of the settling chamber as done in Eq. 21. At the inlet of the settling chamber a fully reflective mass flow inlet is used, as for the numerical simulation, giving,

$$R_{in} = \left(\frac{1 - M_{in}}{1 + M_{in}}\right) \exp(-2\pi i f \frac{L_{in}}{c_1(M_1 + 1)}) \exp(-2\pi i f \frac{L_{in}}{c_1(1 - M_1)}) \quad , \tag{27}$$

where M_{in} and M_{sc} are the Mach numbers at the inlet and inside of the settling chamber respectively. It can be seen that for small frequencies R_{in} tends to $(1 - M_{in})/(1 + M_{in})$, and knowing that M_{in} is small, we obtain $R_{sc} \approx 1$. Using the numerical simulations the reflection coefficient can be calculated, showing a good agreement with the model.

3. Propagation

The propagation of waves through the nozzle of the EWG can be computed analytically in the low frequency limit [2] by writing the jump conditions through the nozzle using the compact nozzle hypothesis. This assumption states that the characteristic wavelength of the waves propagating through the nozzle λ is long compared to the nozzle length. In other words, the Helmholtz number (or dimensionless frequency),

$$\Omega = \frac{L_n}{\lambda} = \frac{f L_n}{c_1} \quad , \tag{28}$$

is negligible. $L_n = 263$ mm is the nozzle length, c_1 is the sound speed at the inlet section of the nozzle (see Fig. 2) and f the frequency. For the EWG experiment, Fig. 3 shows that most of the spectral energy of the temperature pulse is contained at frequencies lower than 100 Hz, which gives a maximum Helmholtz number of $\Omega \approx 0.077$, so that the compact nozzle assumption is apparently reasonable. As the wavelength of the perturbations is long compared to the nozzle length, it can be assumed that the perturbations are transmitted from the inlet to the outlet with no time delay. The conservation equations of mass, enthalpy and entropy can be written as a simple jump condition for

the fluctuations between the inlet and the outlet of the nozzle as done for the heating device,

$$\left(\frac{\dot{m}'}{\dot{m}}\right)_1 = \left(\frac{\dot{m}'}{\dot{m}}\right)_2 \quad , \tag{29}$$

$$\left(\frac{T_t'}{T_t}\right)_1 = \left(\frac{T_t'}{T_t}\right)_2 \quad , \tag{30}$$

$$\left(\frac{s'}{C_p}\right)_1 = \left(\frac{s'}{C_p}\right)_2 \quad . \tag{31}$$

These jump conditions are written as a function of the waves through the nozzle (Fig. 8), using Eqs. (8)-(13), to impose the boundary conditions of the nozzle correctly. This yields,

$$(1+\frac{1}{M_1})P_1^+ + (1-\frac{1}{M_1})P_1^- = (1+\frac{1}{M_2})P_2^+ + (1-\frac{1}{M_2})P_2^- \quad , \tag{32}$$

$$\frac{(1+M_1)P_1^+ + (1-M_1)P_1^- + \dfrac{\sigma_1}{\gamma-1}}{1+\dfrac{\gamma-1}{2}M_1^2} = \frac{(1+M_2)P_2^+ + (1-M_2)P_2^- + \dfrac{\sigma_2}{\gamma-1}}{1+\dfrac{\gamma-1}{2}M_2^2}, \tag{33}$$

$$\sigma_1 = \sigma_2 \quad . \tag{34}$$

For the subsonic case, three waves are incoming (P_1^+, σ_1 and P_2^-) and have to be imposed, and three are out-coming, and therefore unknown (P_1^-, P_2^+ and σ_2), as seen in Fig. 8. The problem can be solved using the three relations of Eq. (32)-(34), the incoming waves of Eqs. (17)-(19) and the reflection coefficients R_1 and R_2 calculated in Section III B 2.

The downstream propagating acoustic wave at the inlet (P_1^+) is calculated as the sum of the reflected wave and the total acoustic wave generated by the heating device at the inlet of the nozzle,

$$P_1^+ = R_1 P_1^- + P_h \quad . \tag{35}$$

The acoustic wave P_h represents the direct noise source term, and is calculated as the combination of both acoustic waves generated by the heating device (P_h^+ and P_h^-, using Eqs.(18)-(19)) using the inlet reflection coefficient. Knowing that $q' = \sigma_h$, it reads,

$$P_h = P_h^+ + R_1 \cdot P_h^- = \frac{1}{2}\left(\frac{M_1}{M_1+1} + R_1\frac{M_1}{1-M_1}\right)\sigma_h \quad . \tag{36}$$

A matrix system can be written to solve the problem considering both reflecting coefficients at the inlet and outlet of the nozzle R_1 and R_2,

$$\begin{bmatrix} R_1 & -1 & 0 & 0 \\ 0 & 0 & -1 & R_2 \\ \xi_1^- & \xi_1^+ & -\xi_2^- & -\xi_2^+ \\ \zeta_1\beta_1^- & \zeta_1\beta_1^+ & -\zeta_2\beta_2^- & -\zeta_2\beta_2^+ \end{bmatrix} \begin{bmatrix} P_1^- \\ P_1^+ \\ P_2^- \\ P_2^+ \end{bmatrix} = \begin{bmatrix} 0 \\ 0 \\ 0 \\ \zeta_2 - \zeta_1 \end{bmatrix} \sigma_1 - \begin{bmatrix} 0 \\ 0 \\ \xi_1^+ \\ \zeta_1\beta_1^+ \end{bmatrix} P_h \quad , \tag{37}$$

which can be reduced into a more compact form,

$$\begin{bmatrix} \xi_1^+ R_1 + \xi_1^- & -(\xi_2^+ + \xi_2^- R_2) \\ \\ \zeta_1(\beta_1^+ R_1 + \beta_1^-) & -\zeta_2(\beta_2^+ + \beta_2^- R_2) \end{bmatrix} \begin{bmatrix} P_1^- \\ \\ P_2^+ \end{bmatrix} = \begin{bmatrix} 0 \\ \\ \zeta_2 - \zeta_1 \end{bmatrix} \sigma_1 - \begin{bmatrix} \xi_1^+ \\ \\ \zeta_1\beta_1^+ \end{bmatrix} P_h \quad , \tag{38}$$

where ξ, β and ζ are a function of the Mach number only,

$$\xi^{\pm} = 1 \pm \frac{1}{M} \quad , \tag{39}$$

$$\beta^{\pm} = (\gamma - 1)(1 \pm M) \quad , \tag{40}$$

$$\zeta = \left(1 + \frac{\gamma - 1}{2} M^2\right)^{-1} \quad . \tag{41}$$

The problem is solved using the Fourier transform of the source terms and solving the matrix system to find P_1^- and P_2^+ for each frequency. The pressure signal is obtained inverting Eqs. (11)-(12) as,

$$p'_{micro} = (\gamma p_2)\left(P^+_{micro} + P^-_{micro}\right) \quad , \tag{42}$$

and calculating the inverse Fourier transform. The subscript *micro* makes reference to the location of the microphone. The waves at the microphone location can be calculated with a simple phase-shift, $P^+_{micro}(x) = P_2^+ \exp[-2\pi i f x/(c_2(1+M_2))]$ and $P^-_{micro}(x) = P_2^- \exp[-2\pi i f x/(c_2(1-M_2))]$.

In Eq. (38), the two source terms σ_1 and P_h are related to the indirect and the direct source terms respectively. To study the influence of indirect noise only, it is sufficient to set the other term to zero. An alternative method to solve the problem has also been proposed by Bake *et al.* [13] considering no reflection coefficients and only indirect noise. This method is described in

the appendix.

Figure 9 shows the results obtained using only the indirect source term (setting P_h to zero). Neither the shape nor the amplitude of the signal are correctly predicted. It should be noticed that the experimental noise level is 20 times larger than the predicted one and that the reflection coefficients should be taken into account to reproduce the experiment, as they have a strong influence on the signal.

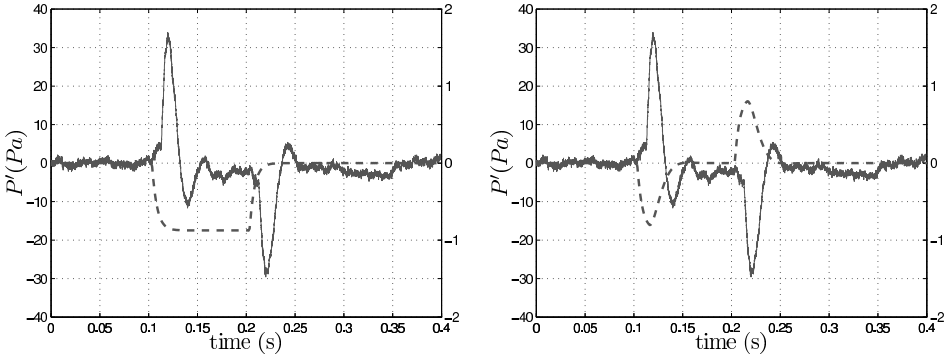

(a) Non-reflecting outlet ($R_2 = 0$) (b) Partially reflecting outlet

Fig. 9 Experimental pressure signal obtained at the outlet microphone (X_{mic} = 1150 mm) compared to the analytical results considering indirect noise generation only (σ_1, while $P_h = 0$). Solid line: Experimental data (left scale), Dashed line: Analytical method (right scale).

Figure 10 shows the solution of Eq. (38) with all source terms when using a non reflecting inlet and outlet boundary conditions ($R_1 = 0$, $R_2 = 0$) (Fig. 10(a)), a non-reflecting inlet and a partially reflective outlet ($R_1 = 0$, $R_2 \neq 0$) (Fig. 10(b)) and a reflecting inlet and outlet ($R_1 \neq 0$, $R_2 \neq 0$) (Fig. 10(c)).

The results show a good agreement when considering all reflection coefficients and both direct and indirect noise, though the peak values are over-predicted. The comparison of Fig. 9 and Fig. 10 shows that the influence of direct noise is stronger than the indirect noise. To illustrate the order of magnitude of both contributions, the indirect to direct noise ratio is considered and defined as in [9],

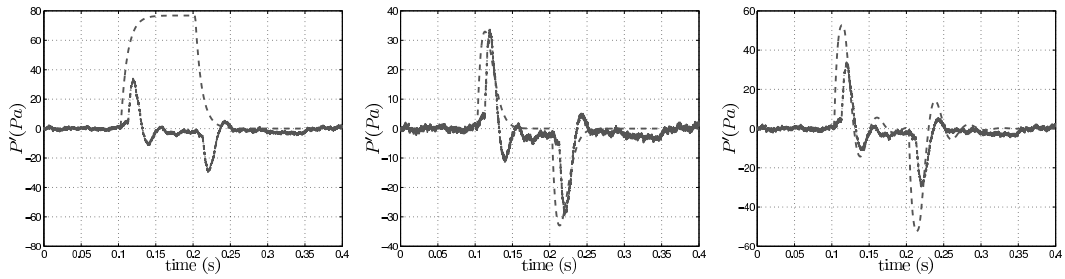

(a) Non-reflecting inlet ($R_1 = 0$) and outlet ($R_2 = 0$)

(b) Non-reflecting inlet ($R_1 = 0$) and partially reflecting outlet

(c) Reflecting inlet and outlet

Fig. 10 Experimental pressure signal obtained at the outlet microphone ($X_{mic} = 1150$ mm) compared to the analytical results considering both direct (P_h) and indirect (σ_1) noise. Solid line: Experimental data, Dashed line: Analytical method.

$$\eta = \frac{P^+_{2,ind}}{P^+_{2,dir}} = \underbrace{\left[\frac{P^+_{2,ind}}{\sigma_1}\right]}_{\text{Indirect noise ratio}} \times \underbrace{\left[\frac{\sigma_h}{P^+_h}\right]}_{\text{Wave ratio}} \times \underbrace{\left[\frac{P^+_{2,dir}}{P^+_1}\right]^{-1}}_{\text{Direct Noise ratio}} . \tag{43}$$

It represents the ratio between the acoustic waves generated at the outlet of the nozzle by indirect mechanisms, and those generated by direct ones. The 'Wave ratio' is the ratio between entropy and acoustic waves generated by the heating device (obtained by dividing Eqs. (17)-(18)), giving,

$$\left[\frac{\sigma_h}{P^+_h}\right] = 2\frac{1+M_1}{M_1} \quad . \tag{44}$$

The indirect ($P^+_{2,ind}/\sigma_1$) and the direct ($P^+_{2,dir}/P^+_1$) noise ratio terms of Eq. (43) are the transfer functions of the nozzle. They are both calculated analytically using Eqs. (32)-(34): to calculate the indirect noise ratio, an entropy wave is considered while all other incoming waves are set to zero, and for the direct noise ratio only an incoming acoustic wave P^+_1 is considered,

$$\left[\frac{P^+_2}{\sigma_1}\right] = \frac{M_2 - M_1}{1+M_2}\frac{\frac{1}{2}M_2}{1+[(\gamma-1)/2]M_2M_1} \quad , \tag{45}$$

$$\left[\frac{P^+_2}{P^+_1}\right] = \frac{2M_2}{1+M_2}\frac{1+M_1}{M_1+M_2}\frac{1+[(\gamma-1)/2]M_2^2}{1+[(\gamma-1)/2]M_2M_1} \quad . \tag{46}$$

The noise ratio gives $\eta \approx 10^{-2}$, showing that indirect noise is negligible compared to direct

noise, and that the measured pressure waves at the outlet are not caused by entropy waves but rather by the acoustics generated by the heating device.

C. SNozzle method

As stated before, the compact nozzle hypothesis is strictly valid only in the limit of infinite wavelength (zero frequency), though it has been used for small but non-zero frequencies. Leyko *et al.* [9] showed that this assumption gives correct results for dimensionless frequencies up to $\Omega = 0.2$ in the case of supersonic nozzles and subsonic convergent nozzles, but the case of a subsonic convergent divergent nozzle has never been considered. Bake *et al.* [13] suggest that the compact nozzle hypothesis is no longer valid when considering a convergent-divergent flow and therefore that the results shown in Section III B might be misleading. Indeed the analytical equations obtained with the compact nozzle hypothesis (Eqs. (32)-(34)) only take into account inlet to outlet relations, regardless of the flow evolution through the nozzle. In the reference case studied in this paper, the inlet and outlet Mach numbers are low, but the nozzle Mach number is large and the strong acceleration/deceleration produced inside the nozzle is not taken into account by the analytical model.

To study the validity of the compact assumption for non-zero frequencies in this type of nozzles, a numerical code based on the developments of Lamarque *et al.* [19] called SNozzle will be used. The code solves the linearized Euler equations in the frequency domain, imposing the incoming waves, and using non-reflecting boundary conditions. The linearized Euler Equations (LEE) are written as,

$$\left[\frac{\partial}{\partial t} + u\frac{\partial}{\partial x}\right]\left(\frac{p'}{\gamma p}\right) + u\frac{\partial}{\partial x}\left(\frac{u'}{u}\right) = 0 \quad , \tag{47}$$

$$\left[\frac{\partial}{\partial t} + u\frac{\partial}{\partial x}\right]\left(\frac{u'}{u}\right) + \frac{c^2}{u}\frac{\partial}{\partial x}\left(\frac{p'}{\gamma p}\right) + \left(2\frac{u'}{u} - (\gamma-1)\frac{p'}{\gamma p}\right)\frac{du}{dx} = \frac{du}{dx}\frac{s'}{C_p} \quad , \tag{48}$$

$$\left[\frac{\partial}{\partial t} + u\frac{\partial}{\partial x}\right]\left(\frac{s'}{C_p}\right) = 0 \quad , \tag{49}$$

The indirect noise is caused by the last term of Eq. (48), where the entropy wave appears as a source term, which is non-zero when a mean flow gradient exists. The amplitude of the indirect

noise directly depends on the mean flow acceleration, which is not seen by the analytical model, as it considers only a jump condition between the inlet and the outlet. The time derivatives are replaced by $2\pi if$ as the equations are solved in the frequency domain. Spatial derivatives are discretized with a central differencing scheme on a staggered 1D grid to prevent checkerboard oscillations.

The code is used to solve for the direct ($P^+_{2,dir}/P^+_1$) and indirect ($P^+_{2,ind}/\sigma_1$) noise ratios of Eqs. (45)-(46) in the SNozzle domain of Fig. 2 without the compact nozzle hypothesis. Results are plotted in Fig. 11 as a function of the reduced frequency for the EWG nozzle geometry. The compact nozzle solution (shown as a symbol) is only correct for the limit of very small Helmholtz numbers as the indirect noise ratio increases fast with frequency. From $\Omega \approx 0.03$ to the maximum dimensionless frequency of the signal ($\Omega \approx 0.077$), the indirect noise ratio is 20 times larger than the one predicted using the analytical method. The following physical interpretation is proposed: when considering zero-frequency, the entropy wave entering the nozzle generates a strong acoustic wave in the convergent, and another one in the divergent. These two waves have opposite phases due to the mean flow acceleration term in Eq. (48) (which is positive in the convergent, and negative in the divergent), and they cancel out at the outlet when they are added up, giving a small global contribution. When a non-zero frequency wave is considered, the phase-shift of both waves is not exactly π as the propagation of the waves through the nozzle has to be taken into account. Due to this change of phase, the two strong acoustic waves do not cancel out completely, generating an extra contribution due to the convergent-divergent effect. This extra contribution cannot be modelled by the compact nozzle method, as it takes into account only the global acceleration between the inlet and the outlet. This effect does not occur when the flow is only accelerated (or only decelerated).

The indirect to direct noise ratio calculated using SNozzle transfer functions is shown in Fig. 12. For the frequency range of interest ($\Omega < 0.077$), this ratio increases significantly, but the indirect noise is still smaller than direct noise, and therefore the direct noise generation cannot be neglected as already shown by the analytical method in Section III B.

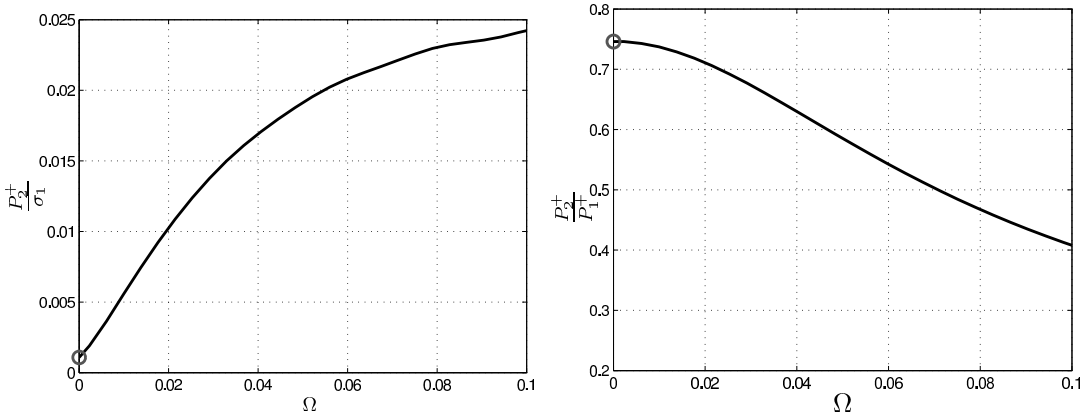

(a) Indirect noise ratio

(b) Direct noise ratio

Fig. 11 Nozzle transfer functions calculated using SNozzle. Symbol: Analytical solution ($\Omega = 0$). Solid line: SNozzle code solving Eqs. 47-49.

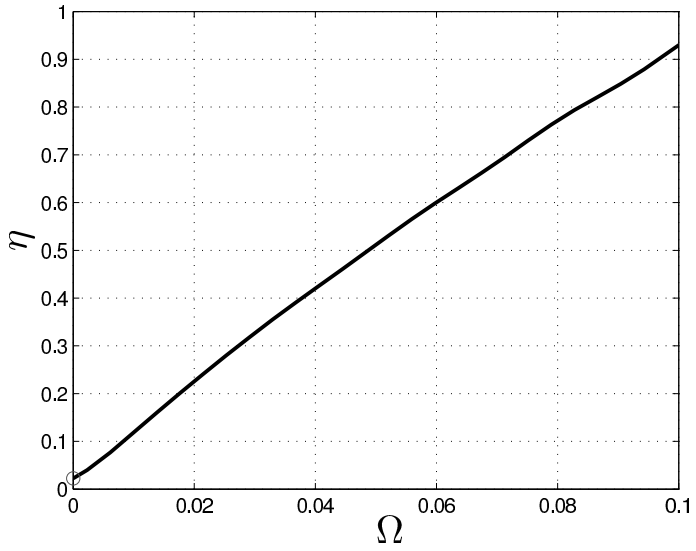

Fig. 12 Indirect to direct noise ratio η (Eq 43). Dot: Analytical solution ($\Omega = 0$). Solid line: SNozzle solution solving the LEE (Eqs. 47-49).

The large differences observed between the compact and the non-compact solutions at small reduced frequencies in Fig. 11 suggest that the compact nozzle hypothesis can be a source of error for convergent-divergent subsonic nozzles as the EWG. The code SNozzle has then been used to develop a semi-analytical method to calculate the pressure signal at the exit of the nozzle without the compact nozzle hypothesis. The propagation equations of the analytical method will be replaced

by the transfer functions of the nozzle, calculated using the 1D LEE code SNozzle in the restricted 'SNozzle domain' plotted in Fig. 2. This will be combined with the same reflection coefficients at the inlet and the outlet as in Section III B and the same analytical model for the heating device. In this way the non-compactness of the nozzle alone can be assessed accurately. To yield the complete semi-analytical model, the transfer functions, defined as the out-coming waves generated by a unitary incoming wave, are calculated using non reflecting boundary conditions at all boundaries. Combining the incoming and out-coming waves, nine transfer functions are then obtained, namely,

$$\left[\frac{P_1^-}{P_1^+}\right] \quad , \quad \left[\frac{P_1^-}{\sigma_1}\right] \quad , \quad \left[\frac{P_1^-}{P_2^-}\right] \quad , \tag{50}$$

for the upstream propagating acoustic wave,

$$\left[\frac{P_2^+}{P_1^+}\right] \quad , \quad \left[\frac{P_2^+}{\sigma_1}\right] \quad , \quad \left[\frac{P_2^+}{P_2^-}\right] \quad , \tag{51}$$

for the entropy wave, and,

$$\left[\frac{\sigma_2}{P_1^+}\right] \quad , \quad \left[\frac{\sigma_2}{\sigma_1}\right] \quad , \quad \left[\frac{\sigma_2}{P_2^-}\right] \quad , \tag{52}$$

for the downstream propagating acoustic wave. These transfer functions are frequency-dependent. To calculate them, three sets of simulations were performed using SNozzle. In each one, a single unitary wave (entropy σ_1, acoustic at the inlet P_1^+ or acoustic at the outlet P_2^-) is introduced to calculate the out-coming ones. For each set of simulations, a frequency sampling was done. In this way each SNozzle simulation has a single unitary incoming wave at a single frequency and the transfer functions of Eqs. (50)-(52) can be calculated independently as a function of frequency. The results obtained are used to solve the EWG problem including the waves and reflection coefficients. The linear property of the LEE solution is first used to write,

$$P_1^- = \left[\frac{P_1^-}{P_1^+}\right] \cdot (P_1^+ + P_h) + \left[\frac{P_1^-}{\sigma_1}\right] \cdot \sigma_h + \left[\frac{P_1^-}{P_2^-}\right] \cdot P_2^- \quad , \tag{53}$$

$$P_2^+ = \left[\frac{P_2^+}{P_1^+}\right] \cdot (P_1^+ + P_h) + \left[\frac{P_2^+}{\sigma_1}\right] \cdot \sigma_h + \left[\frac{P_2^+}{P_2^-}\right] \cdot P_2^- \quad , \tag{54}$$

Writing the acoustic waves at the inlet and at the outlet as $P_1^+ = R_1 \cdot P_1^-$ and $P_2^- = R_2 \cdot P_2^+$, two extra equations are obtained. The system can be re-arranged in a matrix form as,

$$\begin{bmatrix} R_1 & -1 & 0 & 0 \\ 0 & 0 & -1 & R_2 \\ 0 & \left[\frac{P_2^+}{P_1^+}\right] & \left[\frac{P_2^+}{P_2^-}\right] & -1 \\ -1 & \left[\frac{P_1^-}{P_1^+}\right] & \left[\frac{P_1^-}{P_2^-}\right] & 0 \end{bmatrix} \begin{bmatrix} P_1^- \\ P_1^+ \\ P_2^- \\ P_2^+ \end{bmatrix} = \begin{bmatrix} 0 \\ 0 \\ -\left[\frac{P_2^+}{\sigma_1}\right] \\ -\left[\frac{P_1^-}{\sigma_1}\right] \end{bmatrix} \sigma_h + \begin{bmatrix} 0 \\ 0 \\ -\left[\frac{P_2^+}{P_1^+}\right] \\ -\left[\frac{P_1^-}{P_1^+}\right] \end{bmatrix} P_h \quad . \tag{55}$$

This system of equations is similar to the analytical one given above. Eq. (37) can be recovered if the numerical transfer functions are replaced by the analytical compact formula. The matrix and the source terms are all frequency-dependent, therefore the system has to be solved using the Fourier transform of the signal. The pressure signal at the microphone is again obtained with Eq. (42).

The experimental data is compared to the semi-analytical method in Fig. 13: no significant differences are observed. This suggests that the direct noise generated by the EWG experiment can be considered compact. Like for the numerical results of Fig. 6, the differences that can be still observed between the semi-analytical method and the experimental results are probably due to the modelling of the boundary conditions, especially the inlet reflection coefficient (R_1), where no experimental data is available.

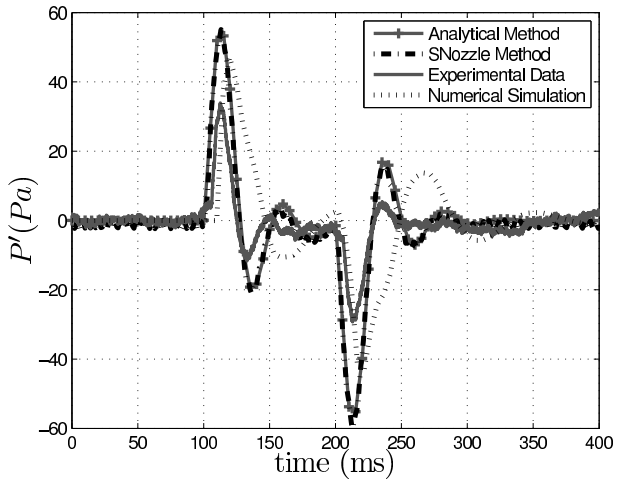

Fig. 13 Pressure signal measured at the outlet for Reference Test Case 2 (Mach 0.7 at the throat). Solid line: Experimental data. Grey dashed line: Numerical simulations. Dark dashed line: Marble and Candel Method. Red dashed line: SNozzle method.

IV. Results for different nozzle Mach numbers

Section III has shown that the analytical method of Section III B and the semi-analytical approach of Section III C were able to reproduce the wave transmission in the EWG setup for subsonic cases when all reflection coefficients are accounted for. Both methods are now used to reproduce the experimental data for different nozzle Mach numbers. In Fig. 14 the maximum value of the pressure fluctuation is compared to the experimental data [13] for several nozzle Mach numbers. Both present methods predict the slope better than the DLR analytical model though they over-predict the peak value of the pressure signal significantly. Both methods still fail to predict the decrease of noise at higher Mach numbers. This decrease is probably caused by the reflecting coefficients: as seen when comparing Figs. 10(a)-10(c), the pressure signal observed should be significantly stronger if there was no reflection of the waves at the outlet. This means that an exact boundary condition should be imposed at the inlet (R_1), where for the moment no experimental data exists. Another hypothesis could be the viscous effects and the vortex-shedding at the divergent of the nozzle, as proposed by Howe [3].

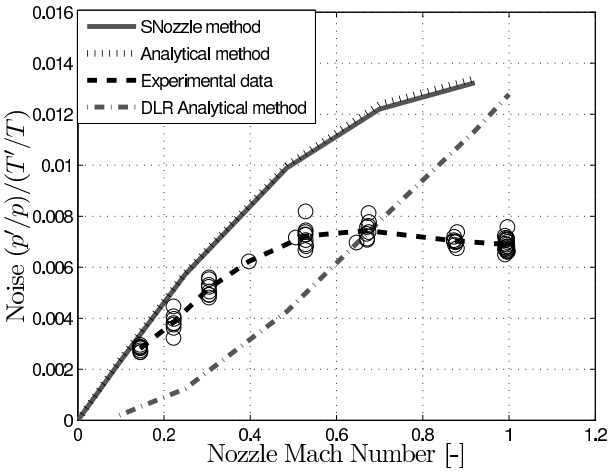

Fig. 14 Evolution of the noise peak at the outlet of the EWG as a function of the throat Mach number.

V. Conclusions

The subsonic case of the EWG experiment performed at DLR has been studied using three different methods: numerical simulations of the Euler equations, analytical solution with Marble

and Candel's model and the quasi one-dimensional linearized Euler equations model in the frequency domain. The direct noise has been shown to have an important effect on the global noise generated: the noise measured at the outlet comes from both direct and indirect noise generation, and is strongly modified by the reflection at the boundaries of the experimental set-up. The fully analytical model, based on the compact nozzle hypothesis, correctly predicts the shape of the pressure signal at the outlet when all reflection coefficients are included, but overpredicts the peak amplitude. The LEE code (SNozzle) shows that the limits of the analytical model to predict the indirect and direct noise generation for non-zero frequencies in this configuration may be caused by the compactness assumption in Marble and Candel's model which is no longer valid in the subsonic case for large frequencies. Successive stages of subsonic acceleration and deceleration of the mean flow are present in axial turbo-machines, and therefore a detailed study of these cases should be made to analyse the possible errors made when using the compact nozzle hypothesis to calculate the noise at the outlet of aero-engines. A semi-analytical method where the LEE solver is used to compute the transfer functions of the nozzle has been used to solve the propagation through the nozzle without the compact nozzle hypothesis with a strict separation of direct and indirect noise and taking into account the inlet and outlet reflection coefficients. This method gives the right trend for the reference test case and over a wide range of throat Mach numbers for the first time. It also shows that the direct noise generated in the EWG experiment can be considered compact and can be calculated using Marbel and Candel's analytical theory at low Mach numbers. However at larger Mach numbers the pulse generated by the heating device may shift towards higher frequencies as suggested by Howe [3], where non-compact effects are larger and tend to reduce the direct noise as seen in Fig. 11b. Using a first order analysis of the waves generated by the heating device it has been shown that, for the subsonic cases, direct noise is significant in the experimental set-up and that the indirect noise is negligible compared to it. The level of direct noise is even emphasized by the inlet reflection. These results differ from the choked case of [12] where indirect noise dominated direct noise.

Appendix

To study the subsonic convergent divergent nozzle, a method was proposed by Bake *et al.* [13] to solve the propagation analytically using the compact nozzle hypothesis without the limitations of Marble and Candel's theory. This method is based on the division of the nozzle into two subsonic nozzles, one convergent and another one divergent. To solve the propagation of the waves, the quasi-transfer functions of the nozzle is calculated separately for the convergent and for the divergent and the propagation is studied sequentially. Yet this combination of transfer functions is actually coupled: the noise generated in the convergent depends on the reflection of the waves in the divergent, and vice versa. To solve the system of equations, Bake *et al.* [13] thus neglected the upstream propagating acoustic wave (P_1^-) generated in the divergent (by entropy and acoustic waves). In this way the system of equations is no longer coupled. The quasi-transfer functions obtained can be written in the non-dimensional form using Marble and Candel's method (Eqs. (29)-(31)) between the inlet (1) and the nozzle throat (T) for the convergent, and between the throat and the outlet (2) for the divergent. In the case of the convergent they read,

$$\frac{P_T^+}{P_1^+}[AA] = \frac{2M_T}{1+M_T}\frac{1+M_1}{M_1+M_T}\frac{1+[(\gamma-1)/2]M_T^2}{1+[(\gamma-1)/2]M_TM_1} \quad , \tag{56}$$

$$\frac{P_T^+}{\sigma_1}[SA] = \frac{M_T-M_1}{1+M_T}\frac{\frac{1}{2}M_T}{1+[(\gamma-1)/2]M_TM_1} \quad , \tag{57}$$

$$\frac{\sigma_T}{\sigma_1}[SS] = 1 \quad , \tag{58}$$

and similarly for the divergent, replacing the inlet and throat subscripts for the throat and the outlet respectively. In dimensional form Eqs. (56)-(58) are equivalent to Eqs. (1)-(4) of [13]. The pressure wave at the outlet generated by the entropy wave is calculated combining the transfer functions,

$$\frac{P_2^+}{\sigma_1} = \underbrace{\frac{P_T^+}{\sigma_1}[SA]\cdot\frac{P_2^+}{P_T^+}[AA]}_{\text{Convergent}} + \underbrace{\frac{\sigma_T}{\sigma_1}[SS]\cdot\frac{P_2^+}{\sigma_T}[SA]}_{\text{Divergent}} \quad . \tag{59}$$

The first term is the acoustic wave generated in the convergent which is obtained by the combination of two terms: the indirect noise generation in the convergent, and the propagation of this noise through the divergent. The second term is the indirect noise generated in the divergent, which is obtained combining the propagation of the entropy wave through the convergent with the

indirect noise generation in the divergent.

This method provides the results shown in Fig. 14. It should be noticed that, for this analysis, direct combustion noise and reflecting boundaries were not taken into account. As stated before, the upstream propagating acoustic wave inside the nozzle has been neglected. It can be shown that this wave is significant and has to be included in the analysis. This wave, generated by entropy and acoustic waves propagating through the divergent, generates acoustic waves in the convergent section that propagate downstream contributing to the total noise. To solve the problem, Eq. (29)-(31) can be written between the inlet (1) and the nozzle throat (T), and from the nozzle throat to the outlet (2). We obtain,

$$\left(\frac{\dot{m}'}{\dot{m}}\right)_1 = \left(\frac{\dot{m}'}{\dot{m}}\right)_T = \left(\frac{\dot{m}'}{\dot{m}}\right)_2 \quad , \tag{60}$$

$$\left(\frac{T_t'}{T_t}\right)_1 = \left(\frac{T_t'}{T_t}\right)_T = \left(\frac{T_t'}{T_t}\right)_2 \quad , \tag{61}$$

$$\left(\frac{s'}{C_p}\right)_1 = \left(\frac{s'}{C_p}\right)_T = \left(\frac{s'}{C_p}\right)_2 \quad . \tag{62}$$

If the upstream propagating acoustic wave is not neglected, the method gives the same solution as the analytical solution of Marble and Candel. This occurs because the method proposed is still based on the compact nozzle hypothesis (even if it is applied to two separate elements, the method considers that the distance between them is zero, and the compact nozzle hypothesis could be applied to the whole system). A different solution would be obtained if the distance between the convergent and the divergent is considered different to zero. This last method was tested in the frame of this work, but was found to be too dependent on the considered length.

Acknowledgements

The authors would like to thank Nancy Kings and Friedrich Bake for providing the test case data and fruitful inputs. This work was partly funded by Snecma.

References

[1] F. Bake, C. Richter, B. Muhlbauer, N. Kings, I.Rohle, F.Thiele, and B.Noll. The entropy wave generator (ewg): a reference case on entropy noise. *Journal of Sound and Vibration* , pages 574–598, 2009.

[2] F. E. Marble and S. Candel. Acoustic disturbances from gas nonuniformities convected through a nozzle. *Journal of Sound and Vibration* , 55:225–243, 1977.

[3] M. S. Howe. Indirect combustion noise. *J. Fluid Mech.* , 659:267–288, 2010.

[4] N. A. Cumpsty and F. E. Marble. The interaction of entropy fluctuations with turbine blade rows; a mechanism of turbojet engine noise. *Proc. R. Soc. Lond. A* , 357:323–344, 1977.

[5] M. J. Lighthill. On sound generated aerodynamically. i. general theory. *Proc. R. Soc. Lond. A , Mathematical and Physical Sciences*, 211(1107):564–587, 1952.

[6] T. Colonius, S.K. Lele, and P. Moin. The sound generated by a two-dimensional shear layer: The far field directivity from computations and acoustic analogies. *Computational Aeroacoustics*, 219, 1995.

[7] M. E. Goldstein. A generalized acoustic analogy. *J. Fluid Mech.* , 488:315–333, 2003.

[8] C. Bailly, C. Bogey, and S. Candel. Modelling of sound generation by turbulent reacting flows. *International Journal of Aeroacoustics*, 9(4):461–490, 2010.

[9] M. Leyko, F. Nicoud, and T. Poinsot. Comparison of direct and indirect combustion noise mechanisms in a model combustor. *AIAA Journal*, 47(11):2709–2716, November 2009.

[10] M. Leyko, F. Nicoud, S. Moreau, and T. Poinsot. Numerical and analytical investigation of the indirect noise in a nozzle. In *Proc. of the Summer Program* , pages 343–354, Center for Turbulence Research, NASA AMES, Stanford University, USA, 2008.

[11] M. Leyko, S. Moreau, F. Nicoud, and T. Poinsot. Numerical and analytical investigation of the indirect combustion noise in a nozzle. *Comptes Rendus Mécanique*, 337(6-7):415–425, 2009.

[12] M. Leyko, S. Moreau, F. Nicoud, and T. Poinsot. Numerical and analytical modelling of entropy noise in a supersonic nozzle with a shock. *Journal of Sound and Vibration* , doi:10.1016/j.jsv.2011.01.025, 2011.

[13] F. Bake, N. Kings, A. Fischer, and Rohle I. Experimental investigation of the entropy noise mechanism in aero-engines. *International Journal of Aeroacoustics*, 8(1-2):125–142, 2008.

[14] B. Muhlbauer, B. Noll, and M. Aigner. Numerical investigation of the fundamental mechanism for entropy noise generation in aero-engines. *Acta Acustica united with Acustica 95*, pages 470–478, 2009.

[15] T. Schønfeld and M. Rudgyard. Steady and unsteady flows simulations using the hybrid flow solver avbp. *AIAA Journal* , 37(11):1378–1385, 1999.

[16] L. Selle, F. Nicoud, and T. Poinsot. The actual impedance of non-reflecting boundary conditions: implications for the computation of resonators. *AIAA Journal* , 42(5):958–964, 2004.

[17] T. Poinsot and S. Lele. Boundary conditions for direct simulations of compressible viscous flows. *J. Comput. Phys.* , 101(1):104–129, 1992.

[18] L. Selle, G. Lartigue, T. Poinsot, R. Koch, K.-U. Schildmacher, W. Krebs, B. Prade, P. Kaufmann, and D. Veynante. Compressible large-eddy simulation of turbulent combustion in complex geometry on unstructured meshes. *Combust. Flame* , 137(4):489–505, 2004.

[19] N. Lamarque and T. Poinsot. Boundary conditions for acoustic eigenmodes computation in gas turbine combustion chambers. *AIAA Journal* , 46(9):2282–2292, 2008.